CHINESE OPTICS LETTERS

Vol. 20, No. 6 | June 2022

Perovskite-quantum-dots activated silica fiber X-ray dosimeter

Yuqing Xie (谢玉清)[1], Yue Jing (景 岳)[1], Luyue Niu (牛璐玥)[1], Ci Wang (王 慈)[1], Lei Zhao (赵 雷)[2], Jing Ren (任 晶)[1*], and Jianzhong Zhang (张建中)[1**]

[1] Key Laboratory of In-fiber Integrated Optics, Ministry of Education, Harbin Engineering University, Harbin 150001, China

[2] State Key Laboratory of Particle Detection and Electronics, University of Science and Technology of China, Hefei 230026, China

*Corresponding author: ren.jing@hrbeu.edu.cn

**Corresponding author: zhangjianzhong@hrbeu.edu.cn

Received January 27, 2022 | Accepted March 25, 2022 | Posted Online April 27, 2022

A new type of X-ray fiber dosimeters is proposed that is based on the X-ray response of $CsPbBr_3$ perovskite-quantum-dots (PQDs) activated silica fiber. Such a fiber sensor is constructed by covering a multimode silica fiber with PQDs embedded glass powders using a transparent high-temperature glue. Under X-ray irradiation, the fiber sensor emits bright green light at 525 nm, which can be readily recorded by a CCD spectrometer. The integrated radioluminescence intensity has an excellent linear response to the X-ray dose. Study is given to the fiber sensor concerning its thermal stability in a temperature range of room temperature up to 300°C, resistance to water erosion, and prolonged X-ray irradiation. The results verify that the proposed fiber sensor has the advantages of good thermal stability, chemical durability, and radiation hardness. The studied X-ray fiber sensor holds promise to be used in a real-time, *in-situ*, and remote radiation dose monitoring.

Keywords: perovskite quantum dots; glass ceramics; X-ray radiation; fiber dosimeter.
DOI: 10.3788/COL202220.063401

1. Introduction

X-ray detection technologies have played a crucial role in the fields of medical radiography, non-destructive inspection, high-energy physics research, etc.[1–3]. At present, the X-ray detectors are mainly based on semiconductors and scintillators[4,5]. The semiconductors are extremely sensitive to X-rays and can directly convert X-ray photons into electrons that are collected and read out by an electric circuit. The practical uses of semiconductors, however, are susceptible to electronic interference and sensitivity to temperature. In the case of scintillator-based detectors, X-rays are first converted into visible light by the scintillator [known as radioluminescence (RL)], and then the ultraviolet (UV) or visible light is read out by a photodiode, CCD camera, or photomultiplier tube (PMT). In many cases, the radiation environment is extremely harsh and difficult to access as a result of high temperature, hazardous chemicals, electromagnetic interference, and strong radiation effects—all urgently ask for flexible and remote detection[6,7].

Recently, scintillators attached to the ends of polymethylmethacrylate (PMMA) plastic optical fibers have been implemented to obtain a real-time radiation dose monitoring (on-line dosimetry) at a precise point (punctual evaluation) very distant from the radiation source (remote monitoring)[8–10]. For example, Zhuang *et al.* proposed an embedded structure of a fiber dosimeter by mechanically drilling a hole filled with commercial $Gd_2O_2S:Tb^{3+}$ scintillator powders at the tip of a PMMA fiber[11]. However, plastic fibers suffer from serious degradation at high temperatures and work reliably only below ~100°C. In comparison, inorganic silica-based optical fibers are much more robust than organic counterparts. Balley *et al.* proposed the use of $Y_2O_3:Eu^{3+}$ nanocrystals (NCs) as the scintillator that is coupled to a silica-based fiber for real-time dose rate monitoring in brachytherapy treatment[12]. Girard *et al.* developed a nitrogen-doped silica fiber that can realize detection of various types of irradiations and is capable of dosimetry up to several kilogray (kGy)[13]. Jia *et al.* developed a sensitive dosimeter based on Ce and Tb co-doped $Y_3Al_5O_{12}$ (YAG) crystal-derived fibers[14]. In our previous work, Ce^{3+} and Gd^{3+} co-doped oxyfluoride glass-ceramics were made into fibers for remote radiation detection[7]. All of the aforementioned fibers exhibited good X-ray response and were only limited to varying extent by the complexity in preparation.

Scintillators based on rare earth (RE) ions emitted from 4f–4f forbidden transitions such as Tb^{3+} and Eu^{3+} are endowed with a long RL decay time (several milliseconds). On one hand, a long decay time is favorable for eliminating the Cherenkov interference, and, on the other hand, it sets an unfavorable limit to the sampling frequency[10]. Various scintillators with a fast RL decay time [scale of nanoseconds (ns)] generally activated

by RE ions exhibiting electric-dipole allowed 5d-4f transitions, e.g., $Cs_2HfI_6:Ce^{3+}$, CsI:Tl, $LiYF_4:Ce^{3+}$, CdS, have been used to make fast fiber dosimeters[6,15–18].

The all-inorganic cesium lead halide ($CsPbX_3$, X = Cl/Br/I) perovskites have offered a promising option as a scintillator for X-ray imaging, owing to the following merits: high photoluminescence quantum yield (PLQY, ~90%), fast radiative decay rate (a few tens of ns), good X/γ-ray stopping power, and tunable RL emission wavelengths (well matching a variety of photodetectors)[19]. Significant progress has been made using perovskites in radiation detection. For example, Chen *et al.* reported that all-inorganic perovskite-quantum-dots (PQDs) exhibited a full color tuning ability in the full visible region[20]. Williams *et al.* used PQDs for X-ray imaging and reviewed their prospects as commercial X-ray detectors[21]. Yu *et al.* prepared two-dimensional PQDs as a β-ray scintillator with good heat resistance and radiation hardness[22]. Zhang *et al.* discovered a composite perovskite NC with excellent X-ray imaging resolution, which can be restored to its original state by common heat treatment after being damaged by X-ray irradiation[23].

However, PQDs still confront such an issue as a poor stability when exposed to light, heat, and moisture[17]. By embedding PQDs in an inorganic glass matrix, the stability of PQDs can be greatly improved to the level of meeting practical requirements[24]. Although significant progress has been witnessed in the last few years of using PQDs activated bulk glass scintillators for high-resolution X-rays detection, the fiber-optic dosimeter based on such a scintillator has not yet been reported to the best of our knowledge[25].

In this Letter, we constructed a new type of X-ray fiber dosimeter by coupling tellurite glass powders embedded with $CsPbBr_3$ PQDs as the scintillator with a commercial multimode silica fiber (MMF) as the signal transmission waveguide [see the schematic diagram in Fig. 1(a)]. Experiments have verified that such a fiber dosimeter has a good linear responsiveness and hardness under high-dose X-ray irradiation, as well as a good stability when exposed to high temperature and water erosion. The spatial resolution of X-ray beam intensity is also studied using the proposed fiber sensor.

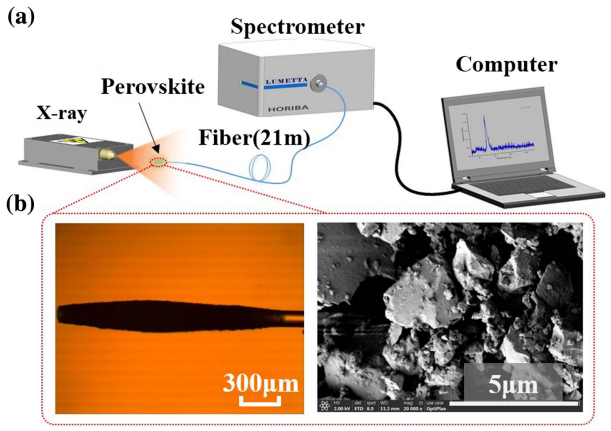

Fig. 1. (a) Schematic diagram of the proposed X-ray detection set-up. (b) Microscopic image of the fiber head covered by PQDs embedded glass powders (left) and scanning electron microscope image of the glass powders (right).

2. Experiments and Methods

The $CsPbBr_3$ PQDs embedded tellurite bulk glass was prepared by the conventional melt-quenching and subsequent thermal treatment method. The detailed preparation procedure can be found elsewhere[24]. Briefly speaking, glass samples with the nominal composition of (in mole percentage) $74.8TeO_2$-$4.4Al_2O_3$-8.8ZnO-4CsBr-$8PbBr_2$-0.5AgCl were prepared using high-purity (99.99%) raw materials purchased from Aladdin (Shanghai, China). An MMF was purchased from YOFC Company (Wuhan, China) with a core diameter of 62.5 μm and a cladding diameter of 125 μm. The refractive indices of the core and the cladding are 1.496 and 1.491, respectively. The numerical aperture is 0.275 ± 0.015.

The micromorphology of powdered glass samples was examined by scanning electron microscopy (SEM, Apreo S, Thermo Scientific). Photoluminescence (PL) emission, PL excitation (PLE), and decay spectra were measured by a PTI QuantaMaster 8000 spectrofluorometer (Horiba, Canada) equipped with a 75 W xenon lamp and a ns pulsed OpoLette355 optical parametric oscillator (OPO) laser (OPOTEK, Canada). X-ray excited RL spectra were recorded by an Omni-A 300i fluorescence spectrometer (Zolix, China) equipped with an X-ray tube (MOXTEK TUB-MAN-1006, the working voltage is up to 60 kV and 12 W, Cu target).

The manufacture of the X-ray fiber sensor is as follows: (i) prepare PQDs embedded glass powders by mechanically grinding the bulk glass in an agate mortar, and the powders thus obtained are of irregular shape and several tens of micrometers in size, as shown in Fig. 1(b); (ii) remove the polymer package from one end of a 21 m long MMF fiber, leaving a 0.2 cm long stripped fiber end; (iii) coat the fiber end with the glass powders using a transparent high-temperature glue (SINWE, UL-94V1, China) with a refractive index of 1.56, forming the X-ray sensitive film of ~65 μm in thickness [Fig. 1(b)]. The coated fiber is then used for X-ray radiation detection. During the measurement, the fiber sensor head was put 1 cm away from the radiation source. The other end of the fiber was connected to a CCD spectrometer (Horiba Lumett) for data reading.

The irradiation dose was expressed by Gy (air), and converted by multiplying the dose rate by the exposure time. The dose rate was measured without a filter by a multifunctional quality testing device of a Barakuda X-ray machine produced by RTI Company. The device consists of a main machine and a multifunctional detector (device number: BC1-08040132 + MPD-08070050). The dose rate was varied by the tube current, and the irradiation time (4 min) was precisely recorded during each run of measurements.

3. Results and Discussion

The PL emission, PLE, and decay spectra of PQDs embedded glass powders were characterized, as shown in Fig. 2. Upon the 365 nm UV excitation, a bright green emission is observed peaking at 525 nm with a narrow bandwidth of ~16 nm, which owes its origin to the bright triplet exciton radiative relaxation of PQDs [Fig. 2(a)][24]. Monitoring the green emission band, a broad excitation band is observed covering the wavelength range of 300–500 nm. Figure 2(b) expresses a double exponential fit to the PL decay curve, based on which the average PL lifetime was calculated to be ~10 ns. The decay rate is typical of PQDs and much faster than commercial $Bi_4Ge_3O_{12}$ (BGO) scintillators (~300 ns), pointing to a good time resolution for imaging uses.

The stability of PQDs embedded glass powders against humidity was checked in a boiling water bath [inset in Fig. 2(c)]. The powders that had been water boiled for 30 min were then measured to compare the changes in the emission spectra and intensity. The whole procedure was repeated six times. As shown in Fig. 2(c), the emission intensity only slightly changes under the repeated measurements, and the deviation in intensity is less than 3.6%, pointing to a good stability again with water erosion. The thermal stability of the powders was also studied under heating (up to 300°C) and cooling (down to room temperature) cycles. The whole process was repeated six times, and the results are shown in Fig. 2(d). Both the emission spectra and the intensity barely change under such treatments, and the deviation in intensity is less than 1%.

The RL spectrum of the PQDs activated silica fiber was measured under X-ray irradiation. Like the UV excitation, a strong and narrow green emission band is observed peaking at 525 nm [Fig. 3(a)][24]. The RL signal was also measured of the fiber not functionalized by PQDs, and no RL signal could be recorded in the PQDs emission wavelength range of 490–560 nm [Fig. 3(a)]. Figure 3(b) shows the relationship between the integrated RL intensity and the radiation dose. The sample was measured three times at each fixed dose, and the averages of the integrated RL intensities were used as the data points. A good linear response to the X-ray dose (in the range of 200 mGy–40 Gy) is revealed by the linear fitting to the experimental data. It is important to note that the RL signal was very stable during the measurement. The burn–bright effect due to filling the trap states was not observed.

Due to the fairly small Stokes shift of $CsPbBr_3$, the self-absorption is inevitable, which sets a fundamental limit to light propagation and amplification. In this work, we only covered a very short length (~2 mm) of the silica fiber by the thin film of $CsPbBr_3$. The light emitted by $CsPbBr_3$ is transmitting in the silica fiber to the spectrometer. The fiber per se is transparent and has limited absorption at the emission wavelength of $CsPbBr_3$. It is noted that there exist some novel perovskite scintillators based on self-trapped excitons with large Stokes shift. For example, Cheng *et al.* proposed a $CsCu_2I_3$ single crystal with a Stokes shift as large as 236 nm[26]. Lian *et al.* prepared $Cs_3Cu_2I_5$ NCs with a high quantum yield and almost zero self-absorption[27]. These materials hold promise in improving the performance of X-ray detection, and the challenge remains to be solved to precipitate such crystals internally in the glass matrix to improve their stability.

To investigate the spatial resolution of X-ray beam intensity, the fiber sensor was fixed on a 3D translation stage and placed

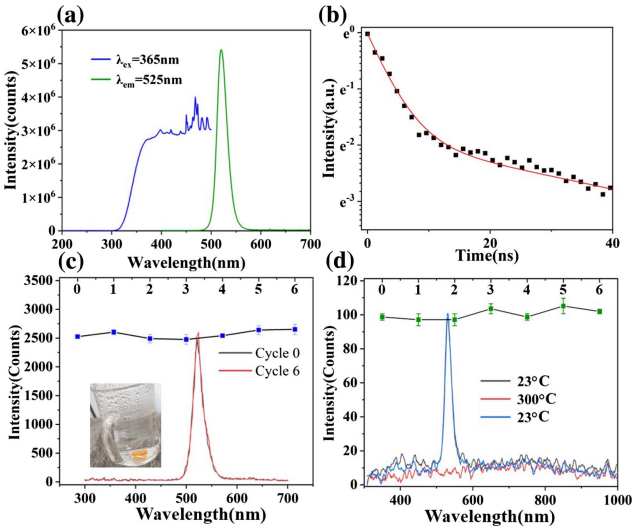

Fig. 2. (a) PL and PLE spectra of PQDs embedded glass powders. (b) PL decay curve and the fit to the data. (c) Variation of emission spectra and intensity under water boiling treatment repeated six times. Inset: glass powders in a boiling water bath. (d) Variation of emission spectra and intensity under heating (up to 300°C)–cooling (down to room temperature) treatment repeated six times.

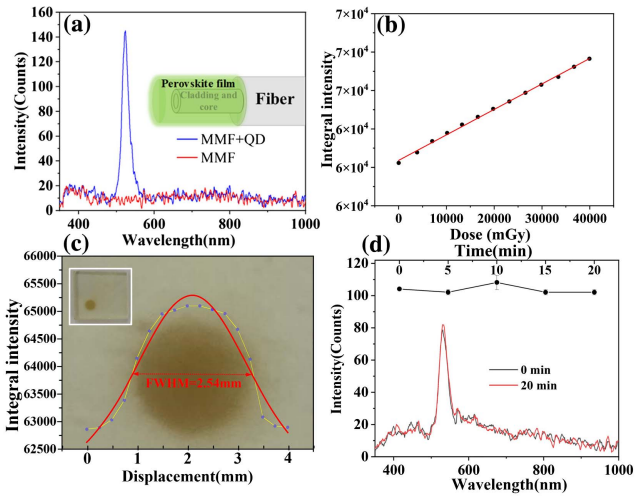

Fig. 3. (a) X-ray excited RL spectra of the PQDs activated silica fiber (blue curve) and the un-coated fiber (red curve). Inset: schematic diagram of the fiber sensor. (b) Relationship between the integrated RL intensity and the X-ray dose. Solid line is the linear fit to the data. (c) Variation of the RL intensity as a function of displacement across the X-ray beams. Red line is the Gaussian fit to the data. Inset: an X-ray sensitive glass used to record the X-ray beam spot. The background is the image of an enlarged spot after X-ray irradiation. (d) Changes in the RL spectra and integrated intensity with X-ray exposure time.

close to the exit aperture of the X-ray tube. The emitted X-ray beam spot has a spatial spread of ~2.5 mm in diameter, as recorded by an X-ray sensitive glass [Ag-doped phosphate glass[28], inset in Fig. 3(c)]. We translated the fiber sensor across the aperture from one edge to the other and recorded the RL spectrum every 250 μm in translational movement. The variation of the integrated RL intensity as a function of displacement is shown in Fig. 3(c). The full width at half-maximum (FWHM) obtained by a Gaussian fitting to the spectrum is 2.54 mm, which is consistent with the spot size recorded using the X-ray sensitive glass. Although we tried to conformally cover the film of PQDs embedded glass powders on the fiber, we still failed to obtain a uniform thickness along the fiber axis [Fig. 1(b)], which could bring some issues with angular dependence.

Finally, the stability of the PQDs activated fiber is examined upon continuous X-ray irradiation. The RL spectrum was recorded every 5 min for up to a total of 20 min. The RL spectra hardly change after the prolonged X-ray exposure with a cumulative dose of 200 Gy. The deviation of the integrated RL intensity before and after the exposure is only about 0.6% [Fig. 3(d)], pointing to an excellent radiation hardness of the proposed fiber sensor.

4. Conclusion

A simple X-ray fiber sensor is constructed by coupling $CsPbBr_3$ PQDs embedded tellurite glass powders with a silica fiber. Capitalizing on the encapsulation of PQDs in the inorganic glass matrix, such a fiber sensor exhibits an excellent thermal stability upon the repeated heating–cooling cycles and a good resistance to water erosion. Benefitting from the strong RL emission from $CsPbBr_3$ PQDs, the fiber sensor shows a good linear response to X-ray dose and can be reliably used upon continuous X-ray irradiation to a total dose of 200 Gy. The fiber sensor is also endowed with a good spatial resolution of the X-rays intensity distribution, and the resolving power is limited only by the fiber diameter.

Acknowledgement

This work was supported by the National Natural Science Foundation of China (No. 51872055), the Fundamental Research Funds for the Central Universities, the State Key Laboratory of Particle Detection and Electronics (No. SKLPDE-KF-202108), and the 111 Project (No. B13015) to the Harbin Engineering University.

References

1. L. Lu, M. Sun, Q. Lu, T. Wu, and B. Huang, "High energy X-ray radiation sensitive scintillating materials for medical imaging, cancer diagnosis and therapy," Nano Energy **79**, 105437 (2021).
2. M. Sytnyk, S. Deumel, S. F. Tedde, G. J. Matt, and W. Heiss, "A perspective on the bright future of metal halide perovskites for X-ray detection," Appl. Phys. Lett. **115**, 190501 (2019).
3. K. Li, Y. Gao, H. Zhang, G. Du, H. Huang, H. Xu, and T. Xiao, "Efficient three-dimensional characterization of C/C composite reinforced with densely distributed fibers via X-ray phase-contrast microtomography," Chin. Opt. Lett. **19**, 073401 (2021).
4. D. Pennicard, B. Pirard, O. Tolbanov, and K. Iniewski, "Semiconductor materials for X-ray detectors," MRS Bull. **42**, 445 (2017).
5. M. Nikl and A. Yoshikawa, "Recent R&D trends in inorganic single-crystal scintillator materials for radiation detection," Adv. Opt. Mater. **3**, 463 (2015).
6. M. Jia, J. Wen, X. Pan, L. Zhang, J. Yuan, Y. Huang, X. Zhang, L. He, F. Pang, and T. Wang, "Flexible scintillation silica fiber with engineered nanocrystals for remote real-time X-ray detection," ACS Appl. Mater. Interfaces **14**, 1362 (2022).
7. B. Sun, Y. Xie, Y. Zhao, X. Li, J. Chen, Y. Song, L. Zhao, Z. Li, H. Zhao, J. Ren, and J. Zhang, "A highly robust Ce^{3+}-doped and Gd^{3+}-mixed $KLaF_4$ nano-glass composite scintillator," J. Mater. Chem. C **9**, 17504 (2021).
8. H. El Hamzaoui, G. Bouwmans, B. Capoen, A. Cassez, R. Habert, Y. Ouerdane, S. Girard, D. Di francesca, N. Kerboub, A. Morana, D. Söderström, A. Boukenter, and M. Bouazaoui, "Gd^{3+}-doped sol-gel silica glass for remote ionizing radiation dosimetry," OSA Contin. **2**, 715 (2019).
9. J. M. Fontbonne, G. Iltis, G. Ban, A. Battala, J. C. Vernhes, J. Tillier, N. Bellaize, C. Le Brun, B. Tamain, K. Mercier, and J. C. Motin, "Scintillating fiber dosimeter for radiation therapy accelerator," IEEE Trans. Nucl. Sci. **49**, 2223 (2002).
10. L. Ding, Q. Wu, Q. Wang, Y. Li, R. M. Perks, and L. Zhao, "Advances on inorganic scintillator-based optic fiber dosimeters," EJNMMI Phys. **7**, 60 (2020).
11. Z. Qin, Y. Hu, Y. Ma, W. Zhao, W. Sun, D. Zhang, Z. Chen, and L. Elfed, "Embedded structure fiber-optic radiation dosimeter for radiotherapy applications," Opt. Express **24**, 5172 (2016).
12. M. D. Belley, O. Craciunescu, Z. Chang, B. W. Langloss, I. N. Stanton, T. T. Yoshizumi, M. J. Therien, and J. P. Chino, "Real-time dose-rate monitoring with gynecologic brachytherapy: results of an initial clinical trial," Brachytherapy **17**, 1023 (2018).
13. S. Girard, D. Di Francesca, A. Morana, C. Hoehr, P. Paillet, C. Duzenli, N. Kerboub, I. Reghioua, G. Li Vecchi, A. Alessi, O. Duhamel, M. Trinczek, E. Marin, A. Boukenter, Y. Ouerdane, J. Mekki, R. Garcia Alia, Y. Kadi, and M. Brugger, "X-Rays, γ-rays, and proton beam monitoring with multimode nitrogen-doped optical fiber," IEEE Trans. Nucl. Sci. **66**, 306 (2019).
14. M. Jia, J. Wen, X. Pan, Z. Xin, F. Pang, L. He, and T. Wang, "Tapered fiber radiation sensor based on Ce/Tb:YAG crystals for remote γ-ray dosimetry," Opt. Express **29**, 1210 (2021).
15. S. Kodama, S. Kurosawa, M. Ohno, Y. Morishita, H. Usami, M. Hayashi, M. Sasano, T. Azuma, H. Tanaka, V. Kochurikhin, A. Yamaji, M. Yoshino, S. Toyoda, H. Sato, Y. Ohashi, K. Kamada, Y. Yokota, A. Yoshikawa, and T. Torii, "Fiber-read radiation monitoring system using an optical fiber and red-emitting scintillator for ultra-high-dose conditions," Appl. Phys. Express **13**, 047002 (2020).
16. M. A. Suarez, T. Lim, L. Robillot, V. Maillot, T. Lihoreau, P. Bontemps, L. Pazart, and T. Grosjean, "Miniaturized fiber dosimeter of medical ionizing radiations on a narrow optical fiber," Opt. Express **27**, 35588 (2019).
17. F. Zhou, Z. Li, W. Lan, Q. Wang, L. Ding, and Z. Jin, "Halide perovskite, a potential scintillator for X-ray detection," Small Methods **4**, 2000506 (2020).
18. C. Wang, H. Lin, Z. Zhang, Z. Qiu, H. Yang, Y. Cheng, J. Xu, X. Xiang, L. Zhang, and Y. Wang, "X-ray excited $CsPb(Cl,Br)_3$ perovskite quantum dots-glass composite with long-lifetime," J. Eur. Ceram. Soc. **40**, 2234 (2020).
19. L. Jiang, X. Luo, Z. Luo, D. Zhou, B. Liu, J. Huang, J. Zhang, X. Zhang, P. Xu, and G. Li, "Interface and bulk controlled perovskite nanocrystal growth for high brightness light-emitting diodes [Invited]," Chin. Opt. Lett. **19**, 030001 (2021).
20. Q. Chen, J. Wu, X. Ou, B. Huang, J. Almutlaq, A. A. Zhumekenov, X. Guan, S. Han, L. Liang, Z. Yi, J. Li, X. Xie, Y. Wang, Y. Li, D. Fan, D. B. L. Teh, A. H. All, O. F. Mohammed, O. M. Bakr, T. Wu, M. Bettinelli, H. Yang, W. Huang, and X. Liu, "All-inorganic perovskite nanocrystal scintillators," Nature **561**, 88 (2018).
21. R. T. Williams, W. W. Wolszczak, X. Yan, and D. L. Carroll, "Perovskite quantum-dot-in-host for detection of ionizing radiation," ACS Nano **14**, 5161 (2020).

22. D. Yu, P. Wang, F. Cao, Y. Gu, J. Liu, Z. Han, B. Huang, Y. Zou, X. Xu, and H. Zeng, "Two-dimensional halide perovskite as β-ray scintillator for nuclear radiation monitoring," Nat. Commun. **11**, 3395 (2020).
23. H. Zhang, Z. Yang, M. Zhou, L. Zhao, T. Jiang, H. Yang, X. Yu, J. Qiu, Y. Yang, and X. Xu, "Reproducible X-ray imaging with a perovskite nanocrystal scintillator embedded in a transparent amorphous network structure," Adv. Mater. **33**, 2102529 (2021).
24. L. Niu, S. Wang, Z. Sui, Y. Song, L. Zhao, L. Liu, J. Ren, and J. Zhang, "Highly stable $CsPbBr_3$ perovskite quantum dot-doped tellurite glass nanocomposite scintillator," Opt. Lett. **46**, 3448 (2021).
25. W. Ma, T. Jiang, Z. Yang, H. Zhang, Y. Su, Z. Chen, X. Chen, Y. Ma, W. Zhu, X. Yu, H. Zhu, J. Qiu, X. Liu, X. Xu, and Y. Yang, "Highly resolved and robust dynamic X-ray imaging using perovskite glass-ceramic scintillator with reduced light scattering," Adv. Sci. **8**, 2003728 (2021).
26. S. Cheng, A. Beitlerova, R. Kucerkova, E. Mihokova, M. Nikl, Z. Zhou, G. Ren, and Y. Wu, "Non-hygroscopic, self-absorption free, and efficient 1D $CsCu_2I_3$ perovskite single crystal for radiation detection," ACS Appl. Mater. Interfaces **13**, 12198 (2021).
27. L. Lian, M. Zheng, W. Zhang, L. Yin, X. Du, P. Zhang, X. Zhang, J. Gao, D. Zhang, L. Gao, G. Niu, H. Song, R. Chen, X. Lan, J. Tang, and J. Zhang, "Efficient and reabsorption-free radioluminescence in $Cs_3Cu_2I_5$ nanocrystals with self-trapped excitons," Adv. Sci. **7**, 2000195 (2020).
28. M. Iwao, H. Takase, D. Shiratori, D. Nakauchi, T. Kato, N. Kawaguchi, and T. Yanagida, "Ag-doped phosphate glass with high weathering resistance for RPL dosimeter," Radiat. Meas. **140**, 106492 (2021).